

Theory and Simulation of Attractive Nanoparticle Transport in Polymer Melts

Umi Yamamoto,^{†,‡} Jan-Michael Y. Carrillo,^{§,¶} Vera Bocharova,^{||,⊙} Alexei P. Sokolov,^{||,⊥} Bobby G. Sumpter,^{§,⊙} and Kenneth S. Schweizer^{*,#,%,&}

[†]Department of Physics, University of Illinois, Urbana, Illinois 61801, United States

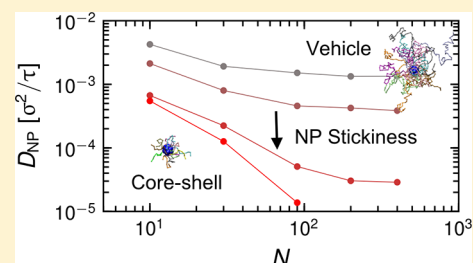
[‡]Division of Chemistry and Chemical Engineering, California Institute of Technology, Pasadena, California 91125, United States

[§]Center for Nanophase Materials Sciences and Computational Sciences & Engineering Division and ^{||}Chemical Sciences Division, Oak Ridge National Laboratory, Oak Ridge, Tennessee 37831, United States

[⊥]Department of Chemistry, University of Tennessee, Knoxville, Tennessee 37996, United States

[#]Department of Materials Science, [%]Department of Chemistry, and [&]Frederick Seitz Materials Research Laboratory, University of Illinois, Urbana–Champaign, Illinois 61801, United States

ABSTRACT: We theoretically study the diffusion of a single attractive nanoparticle (NP) in unentangled and entangled polymer melts based on combining microscopic “core–shell” and “vehicle” mechanisms in a dynamic bond percolation theory framework. A physical picture is constructed which addresses the role of chain length (N), degree of entanglement, nanoparticle size, and NP–polymer attraction strength. The nanoparticle diffusion constant is predicted to initially decrease with N due to the dominance of the core–shell mechanism, then to cross over to the vehicle diffusion regime with a weaker N dependence, and eventually plateau at large enough N . This behavior corresponds to decoupling of NP diffusivity from the macroscopic melt viscosity, which is reminiscent of repulsive NPs in entangled melts, but here it occurs for a distinct physical reason. Specifically, it reflects a crossover to a transport mechanism whereby nanoparticles adsorb on polymer chains and diffuse using them as “vehicles” over a characteristic desorption time scale. Repetition of random desorption events then leads to Fickian long time NP diffusion. Complementary simulations for a range of chain lengths and low to moderate NP–polymer attraction strengths are also performed. They allow testing of the proposed diffusion mechanisms and qualitatively support the theoretically predicted dynamic crossover behavior. When the desorption time is smaller than or comparable to the onset of entangled polymer dynamics, the NP diffusivity becomes almost chain length independent.



I. INTRODUCTION

Nanoparticle (NP) motion in synthetic and biological polymer liquids is of fundamental interest in diverse fields of science and engineering, e.g., for light-weight, easily processable, and low-cost polymer nanocomposites.^{1–3} Transport can be complex since it typically involves multiple time, energy, and length scales.^{1–4} For synthetic polymer melts and concentrated solutions where the polymer–nanoparticle interaction is repulsive, recent experiments^{4–12} and simulations^{13,14} find nanoparticle diffusivity is a rich function of particle size and polymer length scales with large violations of the hydrodynamic Stokes–Einstein (SE) relation. For this problem, Brochard-Wyart and de Gennes¹⁵ pioneered a qualitative scaling approach based on the idea that particle motion becomes “decoupled” from the full macroscopic viscosity when its diameter ($2R$) is smaller than the entanglement mesh size or tube diameter, d_T , for entangled melts or smaller than the polymer radius of gyration (R_g) for unentangled melts. The resulting scaling laws for the particle diffusion constant have been confirmed by simulations^{13,14} for small enough repulsive particles in unentangled melts and lightly entangled melts. A

more advanced scaling approach was constructed and applied to analyze NP diffusion in polymer solutions.¹⁵ For larger NP regimes where $2R/d_T \gtrsim 1$ the possible relevance of hopping as a new mode of transport and intermediate-time diffusion has also been investigated.^{16,17}

The problem of repulsive NP transport has also been quantitatively addressed based on a microscopic, force-level, self-consistent generalized Langevin equation (SC-GLE) theory.^{18,19} It treats in a unified manner the Fickian diffusion of a single repulsive nanoparticle of any size in entangled and unentangled polymer melts. Nanoparticle self-motion and length-scale-dependent polymer relaxation (termed “constraint release”) enter as two parallel and competing channels of force relaxation. For entangled melts, NP long-time mobility exhibits size-dependent non-SE behaviors controlled by (i) fast nanoparticle motion and length-scale-dependent collective relaxation of the unentangled matrix for NPs smaller than the

Received: December 19, 2017

Revised: February 14, 2018

Published: March 8, 2018

tube diameter and (ii) polymer relaxation via reptation for NPs larger than the tube diameter. The two regimes are predicted to be connected by a relatively sharp, but continuous, prehydrodynamic crossover regime at $2R/d_T \approx 1-2$ where NP motion first becomes *gradually* coupled to the entanglement network. Physically, “self-consistent” means the dynamic friction due to polymer forces on a NP can be relaxed via NP motion, but in turn, NP motion is controlled by the relaxation of these same polymer forces. In strong contrast to the analysis of Brochard-Wyart and de Gennes,¹⁵ recovery of hydrodynamic behavior in heavily entangled matrices requires roughly $2R \geq 10d_T$. Theoretical predictions for the diffusion constant are in good agreement with simulations including the crossover regime in lightly entangled melts where $2R \approx d_T$ and experiments in entangled polymer melts and DNA solutions.⁷⁻¹¹

A caveat is that due to its dynamical Gaussian nature, the SC-GLE approach does not address activated hopping transport which has been argued to be relevant in a narrow $2R \approx d_T$ window in strongly entangled liquids and cross-linked networks.¹⁷ This hopping problem has been microscopically addressed using a different theoretical approach, the *non-Gaussian* nonlinear Langevin equation (NLE) theory,²⁰ which predicts it to be important only for a narrow range of $2R/d_T \approx 1.4-1.8$ for heavily entangled melts. The effect of soft repulsive polymer–NP interactions on hopping transport has also been studied.²⁰

Given the above summary of recent theoretical progress, we view the problem of repulsive NP diffusion in polymer liquids to be largely solved, at least at zeroth order. Weak polymer–NP attractions have been treated under the restrictive condition that desorption times are so fast that the polymer–particle adsorbed layer is equilibrated on the time scales required to achieve NP diffusion.¹⁸ In this case, attractive forces only modify local packing of polymers around a NP and local friction in the SC-GLE approach.

The focus of this paper (referred to as paper I) is a combined theoretical and simulation study of how the dilute NP diffusion problem changes if there are strong polymer–particle attractions leading to potentially long-lived adsorption. The time scale of the chemically specific elementary polymer desorption event is crucial, and qualitative changes of NP diffusion relative to the repulsive particle analogue are expected. This problem is of high interest in nanocomposites, which typically require significant polymer–NP attraction to achieve dispersion, and also in diverse biophysical contexts. We are especially interested in the case when the NP is small compared to the polymer radius-of-gyration or (if entangled) the tube diameter. This situation is studied experimentally in the companion paper II.²¹

In section II we develop a theoretical framework for sticky NP diffusion in polymer melts focusing on small particles. Multiple different regimes of parameter dependence are identified in the overall context of two competing transport mechanisms: “core–shell” and “vehicle”. The focus is on qualitative behavior. Section III presents a complementary MD simulation study. A wide range of chain lengths and strength of NP–polymer attraction are studied. The results are interpreted based on the developed theoretical framework. The article concludes with a brief summary in section IV. The Appendix includes additional simulation data.

II. THEORETICAL MODELS FOR THE DIFFUSION OF ATTRACTIVE NANOPARTICLES IN POLYMER MELTS

II.A. Two Competing Mechanisms. We propose that the center-of-mass (CM) diffusivity of a single attractive NP of radius R dissolved in a homopolymer melt involves two distinct nonhydrodynamic microscopic mechanisms we call “core–shell” and “vehicle”. Here we first discuss the qualitative physical picture with the help of the conceptual schematic of Figure 1. On the time scale polymer chains are adsorbed

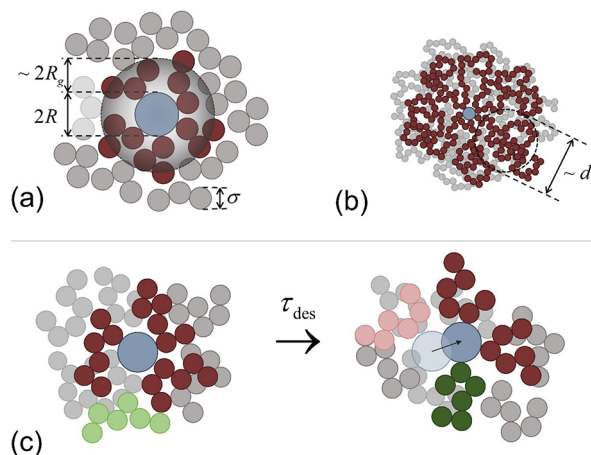


Figure 1. Schematic of one sticky nanoparticle in a polymer melt where matrix chain segments (gray and red circles) are adsorbed onto a NP (blue circle) and (a) the NP radius (R) is larger than radius of gyration (R_g) so that the adsorbed chains (red circles) form a dense layer around a NP creating a core–shell object of effective radius $R_{\text{eff}} \sim R + R_g$ (shaded black region) and (b) $R \ll R_g$ where nonadsorbed segments significantly interpenetrate the adsorbed layer and the effective particle picture breaks down. For entangled melts an additional length scale, the tube diameter (d_T) is indicated. (c) Schematic representation of the “vehicle” mechanism. Initially, a NP follows the adsorbed chain motion (red circles, shown in left panel) using it as carrier or vehicle. This transport mechanism is then randomized by the elementary event of a NP desorbing from a segment and randomly finding a new vehicle chain (green circles, right panel) after a characteristic desorption time, τ_{des} .

(immobilized) on the NP surface, the entity of interest can be viewed as a “core–shell” object. Defining an adsorbed layer thickness as $\sim R_g$, there are two physically distinct limiting regimes: (a) $R \gg R_g$ and (b) $R \ll R_g$. For case (a), the adsorbed shell is essentially space filling, and treating the object as a sphere with an effective hard core radius of $R_{\text{eff}} \sim R + R_g$ is sensible, as argued by others.²²⁻²⁴ But for case (b), non-adsorbed “free matrix” chains can interpenetrate the shell region, rendering a $R_{\text{eff}} \sim R + R_g$ model questionable to a degree that depends on the value of R_g/R and whether polymers are entangled or not.

In both of the above cases, hydrodynamic and nonhydrodynamic effects can enter. The idea of case (a) has been successfully employed to understand the slower than bare ($R_{\text{eff}} = R$) SE diffusion of large silica NPs in poly(2-vinylpyridine) (P2VP).²⁴ The NP diffusivity was found to be in good agreement with the radius-renormalized SE relation

$$D_{\text{SE}} = \frac{k_B T}{6\pi\eta_{\text{full}} R_{\text{eff}}} \quad (1)$$

where k_B is Boltzmann's constant, T is the absolute temperature, and η_{full} is the macroscopic viscosity of the pure polymer liquid. Similar approaches have been employed to describe the NP concentration dependence of the nanocomposite viscosity.^{22,23}

Equation 1 is expected to be sensible only if three conditions apply: (i) case (a) (where $R \gg R_g$) holds, (ii) the segmental desorption time (τ_{des}) is larger than the (a priori unknown) time scale beyond which Fickian diffusion describes NP motion (τ_{diff}), and (iii) nonhydrodynamic effects are weak. Condition (iii) is reasonable for compact core-shell particles larger than microscopic static and dynamic length scales in the polymer liquid. These conditions can be violated if NPs become too small, or polymers become too big, and/or NP-polymer chemistry results in weaker adsorption and a relatively short desorption time. A case of high interest here is when $R < R_g$ and $\tau_{\text{des}} < \tau_{\text{diff}}$; that is, all three of the above conditions are not satisfied. Small sticky NP motion is then expected to be facilitated by the segmental desorption process per a "vehicle" mechanism. Here, the NP moves cooperatively with its local surroundings using polymer chains as carriers, which are temporally renewed on the time scale τ_{des} (see Figure 1c). Repetition of this elementary event randomizes the NP trajectory, allowing long-time Fickian diffusion. Such a vehicle model has been successfully employed to describe single ion diffusion in polymer electrolyte melts^{25,26} where there is strong (but noncovalent) coupling between a cation and polymer backbone. By assuming that the segmental desorption time is independent of chain length, the cation diffusivity was predicted to initially decrease with N but eventually plateaus due to the increased significance of the vehicle mechanism—trends in a good agreement with experiment.^{25,26} However, a general theoretical approach that addresses both variable particle size and entanglement effects has not been established.

Our aim is to develop a more general, but simple, approach for the diffusion of a single attractive NP of any size in unentangled or entangled homopolymer melts by combining the "core-shell" and "vehicle" concepts. It is built on the general framework of dynamic bond percolation theory²⁷ combined with standard Rouse and reptation-tube models for chain and nonlinear polymer melt dynamics^{28,29} and the SC-GLE approach.^{18,19} The problem is rich due to the presence of many length and time scales. In addition to the unknown NP diffusion time τ_{diff} , there is the "bare" NP radius (R), chain radius of gyration (R_g), segmental or alpha relaxation time (τ_0), and polymer-NP desorption time, τ_{des} . For unentangled polymers, the longest chain Rouse relaxation time (τ_R) enters. For entangled melts, there is additionally the entanglement onset time ($\tau_e \approx N_e^2 \tau_0$), reptation time ($\tau_{\text{rep}} \approx (N/N_e) \tau_R$), and tube diameter ($d_T = \sqrt{N_e} b$), where b is the segment length and N_e the entanglement chain length. The polymer melt quantities are typically known, in contrast to τ_{des} . The relative significance of the two diffusion mechanisms is characterized by a competition of the above length and time scales.

II.B. Theoretical Framework. The dynamic bond percolation theory originally developed for diffusion in disordered media²⁷ contains two effects which determine the tagged particle displacement: (i) NP transport via the intermediate-time dynamics of its surroundings and (ii) structural reorganization of the surrounding media which relaxes this coupling. For our problem, (i) corresponds to motion of the core-shell object, while (ii) corresponds to the

desorption event that replaces the old polymer vehicle with a new vehicle. In its simplest implementation, the latter is treated in a Markovian manner (no memory) so that the NP trajectory becomes decorrelated with its past after a single desorption event. In the context of the SC-GLE theory, the total NP-polymer force time correlation function effectively relaxes on the single desorption event time scale. Of course, while a NP is associated with a vehicle, memory effects can be present in the sense that NP motion is slaved to subdiffusive polymer motions on short enough time scales.

The above approximate framework implies that the long-time NP diffusivity follows from its mean-square displacement (MSD), $\langle \delta \vec{r}^2(t) \rangle$, as:²⁷

$$D_{\text{NP}} = \lim_{t \rightarrow \infty} \frac{\langle \delta \vec{r}^2(t) \rangle}{6t} = \frac{1}{6\tau_{\text{des}}} \int_0^\infty dt \langle \delta \vec{r}^2(t) \rangle_0 P_{\text{des}}(t; \tau_{\text{des}}) \quad (2)$$

where a Poisson distribution for the desorption time is employed:

$$P_{\text{des}}(t; \tau_{\text{des}}) = \frac{1}{\tau_{\text{des}}} \exp\left(-\frac{t}{\tau_{\text{des}}}\right) \quad (3)$$

A key input is the MSD of the core-shell object, $\langle \delta \vec{r}^2(t) \rangle_0$, where adsorbed chains are permanently attached. One can then write per standard polymer models^{28,29}

$$\langle \delta \vec{r}^2(t) \rangle_0 = 6D_{\text{core-shell}}t + \mu(t) \quad (4)$$

where $D_{\text{core-shell}}$ is the long-time diffusivity of the core-shell object, and $\mu(t)$ describes its intermediate-time subdiffusive motion. Equations 2 and 4 then yield

$$D_{\text{NP}} = D_{\text{core-shell}} + D_{\text{vehicle}} \quad (5)$$

where the second term is the contribution of the vehicle mechanism to NP diffusivity:

$$D_{\text{vehicle}} \equiv \frac{1}{6\tau_{\text{des}}} \int_0^\infty d\tau \mu(\tau) P_{\text{des}}(\tau; \tau_{\text{des}}) \quad (6)$$

The characteristic time scale for the vehicle diffusivity is given by the average desorption time, τ_{des} , and the corresponding length scale by the nonuniversal average displacement of the core-shell object on the τ_{des} time scale.²⁷ The additive form of eq 5 implies NP diffusivity involves two competing contributions. To calculate D_{NP} requires a model for $D_{\text{core-shell}}$ and $\mu(t)$.

II.C. Core-Shell Diffusivity. We briefly discuss a specific theoretical approach to compute $D_{\text{core-shell}}$. First consider the "large core" regime defined as when $R > R_g$. Here the adsorbed pinned chains form an effectively dense layer that increases the NP radius. In principle, the core-shell object is dynamically coupled with a melt of nonadsorbed chains via hydrodynamic and nonhydrodynamic interactions. To leading order, polymer adsorption enters only via the structure of the adsorbed layer and how it determines an effective repulsive potential between the core-shell object and surrounding polymer matrix. This could be modeled in at least two ways: (i) an effective hard-core interaction with $R_{\text{eff}} \sim R + R_g$ or (ii) an effective hard core plus soft repulsion.²⁰ The bare repulsive NP problem is recovered if segments desorb so fast that they are equilibrated on the NP diffusion time scale.¹⁸

A general way to calculate $D_{\text{core-shell}}$ can be approached based on the SC-GLE theory. For repulsive NPs in entangled and

unentangled melts,^{14,18,19} the starting point of the SC-GLE theory is to express NP diffusivity in an additive form:

$$D_{\text{core-shell}} = D_{\text{hydro}} + D_{\text{non-hydro}} \quad (7)$$

The hydrodynamic contribution is given by the radius-renormalized SE relation (see eq 1), and the nonhydrodynamic contribution follows from the Einstein relation, $D_{\text{non-hydro}} = k_B T / \zeta_{\text{non-hydro}}$ where

$$\zeta_{\text{non-hydro}} = \int_0^\infty dt K(t) \quad (8)$$

and $K(t)$ is the memory function describing the relaxation of the NP–polymer force time correlation function.¹⁸ How the SC-GLE approach describes the physics of this quantity was outlined in the Introduction, and all details are given elsewhere.^{14,18,19}

A useful limiting case is for very large cores ($R \gg R_g$) corresponding to $R_{\text{eff}} \gg 2R_g$. SC-GLE theory then reduces to the radius-renormalized SE result of eq 1 for both unentangled and entangled melts.¹⁸ Moreover, $D_{\text{core-shell}}$ is expected to dominate the net NP diffusion since the vehicle mechanism is irrelevant due to the large separation of relevant length scales.

For the opposite “small core” regime ($R \ll R_g$) the concept of a space-filling core–shell object with $R_{\text{eff}} \sim R + R_g$ breaks down due to the significant interpenetration of nonadsorbed segments into the shell region. The NP motion is then likely sensitive to the dynamics of the adsorbed polymers. Qualitatively, the diffusivity of the pinned core–shell object may be more akin (very crudely) to the dynamics of a starlike polymer (where the NP acts as a branch point) dissolved in a chain melt.^{30,31} For unentangled polymers, the nonhydrodynamic part of $D_{\text{core-shell}}$ can be estimated based on the Rouse model for a starlike polymer in a chain melt:³⁰

$$D_{\text{star}} = \frac{k_B T}{\zeta_0 f N + \zeta_{\text{NP}}} \quad (9a)$$

where ζ_0 is the segmental friction, f is the number of adsorbed chains, and ζ_{NP} is the short-time friction constant of the NP core. For entangled melts, NP diffusion is likely controlled by the constraint release of the surrounding linear chains whence^{30,32}

$$D_{\text{star}} \sim \frac{D_{\text{rep}}(N)}{(N/N_e)^{3/2}} \propto N^{-1} \left(\frac{N_e}{N} \right)^{5/2} D_0 \quad (9b)$$

where $D_0 \equiv k_B T / \zeta_0$ is the segmental diffusion constant and the reptation-tube model diffusivity law is used.^{28,29,33} It is interesting to discuss the relative significance of eqs 9a and eq 9b compared with the corresponding hydrodynamic diffusivities. Given the pinned chains are larger than the core, this is a rather complex problem. If we assume non-free-draining behavior applies on the scale $R_{\text{eff}} \sim R + R_g$, then eq 1 applies which yields the following estimates. For unentangled melts

$$D_{\text{hydro}} = \frac{k_B T}{6\pi\eta_{\text{full}} R_{\text{eff}}} \propto \frac{D_0}{N(R + R_g)} \propto N^{-3/2} \quad (10a)$$

where the final proportionality is valid when $R_g \gg R$. For entangled melts

$$D_{\text{hydro}} \propto \frac{D_0 N_e^2}{N^3 (R + R_g)} \propto \frac{N_e^2}{N^{7/2} D_0} \quad (10b)$$

where the reptation-tube model viscosity is used and the last proportionality assumes $R \ll R_g$. Thus, for both unentangled and entangled melts, it seems the hydrodynamic and nonhydrodynamic contributions to the core–shell diffusivity are small and comparable and decrease more strongly with N compared to the $R > R_g$ regime. This suggests as the polymer size sufficiently exceeds the NP radius, the core–shell diffusivity rapidly decreases with N and tends to play a minor role in the total NP diffusivity.

In summary, we suggest the following scenario for the core–shell diffusivity with decreasing R/R_g . For very large cores ($R \gg R_g$), $D_{\text{core-shell}}$ is described by the radius-renormalized SE relation and dominates the total NP diffusivity. For $R > R_g$, both the hydrodynamic and nonhydrodynamic contributions to $D_{\text{core-shell}}$ can be important. For larger N such that $R < R_g$, the two contributions decrease significantly and likely become irrelevant, leading to a dynamic crossover for sticky NP transport via the vehicle mechanism.

II.D. Vehicle Diffusivity. The sub-diffusive part of the core–shell MSD, $\mu(t)$, which enters D_{vehicle} via eq 5, is generally not possible to calculate exactly except for a few simple cases³⁴ due to the complications of a nonlinear topology of the core–shell, entanglements, nonuniversal consequences of NP–polymer forces, etc. Thus, we focus on a qualitative discussion of leading-order parameter dependences of D_{vehicle} , especially its scaling with N and desorption time. Knowing that the intermediate-time subdiffusive NP motion is controlled by adsorbed segments, $\mu(t)$ is modeled based on the segmental MSD of the adsorbed chains. This can be expressed as

$$\mu(t) = \mu_0 \left(\frac{t}{\tau_0} \right)^\alpha \quad (11)$$

where the subdiffusive exponent, $0 < \alpha < 1$, depends on what regime of polymer dynamics is relevant to NP diffusion. For unentangled melts, and assuming adsorbed chains follow the same segmental dynamics as free chains in the pure melt, one uses the Rouse model to obtain

$$\mu(t) \sim Ab(D_0 t)^{1/2}, \quad \tau_0 < t < \tau_R \quad (12a)$$

$$D_{\text{vehicle}} \approx Ab \left(\frac{D_0}{\tau_{\text{des}}} \right)^{1/2} \quad (12b)$$

where A is a numerical prefactor arising from the core–shell topology. Assuming τ_{des} is determined by the local NP–monomer interaction and is thus N -independent, D_{vehicle} is expected to be (largely) independent of chain length since it is coupled to intermediate-time polymer dynamics and decreases with τ_{des} in contrast to $D_{\text{core-shell}}$. Since we are only interested in large enough τ_{des} such that the subdiffusive polymer segmental motion is relevant, the literal $\tau_{\text{des}} \rightarrow 0$ limit in eq 12a and eq 12b is not considered.

For entangled melts, assuming segmental motion controls the vehicle mechanism, the reptation-tube model^{28,29,33} yields in the asymptotic $N \gg N_e$ limit

$$\mu(t) \approx \begin{cases} b(D_0 t)^{1/2} & t < \tau_e \\ d_T(\sigma^2 D_0 t)^{1/4} & \tau_e < t < \tau_R \\ d_T(D_0 t/N)^{1/2} & \tau_R < t < \tau_{\text{rep}} \end{cases} \quad (13a)$$

$$D_{\text{vehicle}} \approx \begin{cases} Ab \left(\frac{D_0}{\tau_{\text{des}}} \right)^{1/2} & \tau_{\text{des}} < \tau_e \\ Ad_T (b^2 D_0)^{1/4} \left(\frac{1}{\tau_{\text{des}}} \right)^{3/4} & \tau_e < \tau_{\text{des}} < \tau_R \\ Ad_T \left(\frac{D_0}{N \tau_{\text{des}}} \right)^{1/2} & \tau_R < \tau_{\text{des}} < \tau_{\text{rep}} \end{cases} \quad (13b)$$

where A is introduced in the same spirit as in eq 12a. The parameter dependence of the vehicle diffusivity can vary depending on a time-scale competition between τ_{des} , τ_e , τ_R , and τ_{rep} . One expects D_{vehicle} is N -independent if $\tau_{\text{des}} < \tau_R$, while a weak ($\propto N^{-1/2}$) dependence is present for $\tau_R < \tau_{\text{des}} < \tau_{\text{rep}}$. Of course, in the hypothetical long chain limit one can always achieve $\tau_{\text{des}} < \tau_R$ and D_{vehicle} is asymptotically N -independent.

While eqs 12 and 13 can be regarded as the leading-order predictions, there are many well-known nonuniversal features that can change the apparent N scaling of polymer melt dynamics. (i) The exact solution of the Rouse model predicts a weak N -dependence for eq 12b at relatively small N .²⁵ (ii) Segmental diffusivity can depend on N due to the change in glass transition temperature.³⁵ (iii) The $N \gg N_e$ limit often does not apply to experiments or practical simulations. For example, the subdiffusive exponent in the second regime of eq 13a can be N/N_e dependent and approaches 1/4 from above only at very large N/N_e .^{36–38} The second 1/2 exponent regime in eq 13a is very hard to observe unless the system is extremely well entangled.³⁹ In either case, the apparent non-Fickian exponent in eq 11 becomes larger as N/N_e decreases, corresponding to faster than asymptotic segmental motion. Thus, in practice, the parameter dependence of D_{vehicle} is expected to be nonuniversal and should deviate from eqs 12 and 13, including an apparent relatively weak N variation due to nonasymptotic dynamical effects.

II.E. Crossover between Dynamical Regimes. Combining the results of the above subsections, the total NP diffusivity for large $R > R_g$ NPs can be written as

$$D_{\text{NP}} = \frac{k_B T}{c\pi\eta_{\text{full}} R_{\text{eff}}} + \frac{k_B T}{\zeta_{\text{non-hydro}}} + D_{\text{vehicle}} \quad (14a)$$

and for small $R < R_g$ NPs one has

$$D_{\text{NP}} = \frac{k_B T}{c\pi\eta_{\text{full}} R_{\text{eff}}} + D_{\text{star}} + D_{\text{vehicle}} \quad (14b)$$

The additive form of eq 14 suggests that one of the two competing contributions, the core–shell or vehicle diffusivity, likely dominates the NP diffusivity for a given system. Recalling that the N dependence is expected to be weaker for D_{vehicle} , one expects the following crossover behavior at fixed polymer–NP chemistry (τ_{des}).

At sufficiently low N , the core–shell diffusivity makes the dominant contribution to D_{NP} . The NP diffusivity decreases with increasing N until $D_{\text{core-shell}}$ becomes sufficiently reduced that D_{vehicle} begins to dominate. Physically, this behavior can become relevant as $R_g > R$, although the precise crossover condition must be nonuniversal and depends at a minimum on the tube diameter (for entangled melts) and desorption time. Beyond the onset of importance of the vehicle mechanism, the

N -dependence of D_{NP} gradually weakens and for unentangled melts, or entangled melts in the first and second dynamical regimes in eq 13, eventually plateaus as a signature of the vehicle-dominated diffusion mechanism. Although the N -independent diffusivity is reminiscent of the predicted (and observed in simulation) behavior of small repulsive NPs in unentangled and entangled melts,^{13–19} here it arises for different physical reasons. For large enough N , the segmental desorption time (controls decoupling of NP motion from polymer dynamics) can be smaller than the long-time relaxation of the adsorbed chains. Then, the NP diffusivity is only influenced by relatively short or intermediate-time (N -independent to leading order) segmental dynamics. In contrast to the repulsive NP case,^{14–19} the geometric requirement that $2R_{\text{eff}} < d_T$ or $R_{\text{eff}} < R_g$ is formally not present if the desorption time is shorter than the entanglement onset time, although $2R_{\text{eff}} < d_T$ must be satisfied for entangled melts so that the NP transport becomes insensitive to entanglement effects beyond the desorption (vehicle diffusion) time scale.

While nonuniversal aspects can enter in the crossover regime, a generic approach to test the dominance of the vehicle mechanism is to examine whether the following relation holds:

$$D_{\text{NP}}(\tau_{\text{des}})^{1-\alpha} = \text{constant} \quad (N \gg 1) \quad (15)$$

where we assumed $D_{\text{NP}} \sim D_{\text{vehicle}}$ for large N and used eq 13b. Equation 15 formally holds for different choices of τ_{des} with the caveat that α can depend on the relevant polymer dynamics as determined by the competition between τ_{des} , τ_0 , and τ_e . Slowing down of segmental dynamics near the NP surface may also be important depending on the strength of NP–polymer attraction.

The goal of this section was to construct a simple approximate theoretical framework for the diffusion of small sticky nanoparticles in polymer melts. We employ it to qualitatively interpret our simulation results in the following section and experiment in paper II.²¹

III. COARSE-GRAINED SIMULATIONS AND THEORETICAL INTERPRETATION

III.A. Simulation Details. We now study the dynamics of a model attractive NP in unentangled and entangled melts using MD simulation. Besides its intrinsic interest, a major advantage is that several key parameters/quantities that enter the theoretical framework, such as desorption time and time-dependent mean-square displacements, are known, in contrast to experiments. This allows a more incisive test of the theoretical ideas.

We employ the standard coarse-grained bead–spring model⁴⁰ of polymer chains as adopted in ref 14 which studied repulsive NP transport in polymer melts. Nonbonded pair interactions between polymer beads are described by a truncated and shifted Lennard-Jones (LJ) potential with bead diameter σ (used as unit length), spatial cutoff $r_c = 2.5\sigma$, and interaction strength ϵ (in units of thermal energy). The nearest-neighbor bonded interaction is a finite extensible nonlinear elastic (FENE) potential with standard parameters.⁴⁰ A bond bending potential, $U_\theta = k_\theta(1 + \cos \theta)$ with $k_\theta = 0.75 k_B T$, is included to reduce the entanglement chain length, N_e , from 85 to 45; the corresponding tube diameter is $d_T \approx 7-10\sigma$.¹⁴ Initially, several melt simulations with $N = 10, 30, 90, 200$, and 400 are equilibrated using a combination of canonical MD simulations and Monte Carlo bond swaps.⁴¹ During this step,

the nonbonded LJ interactions are switched to an athermal or purely repulsive system by setting $r_c = 2^{1/6}\sigma$.

Nanoparticles are modeled as icosahedrons composed of 12 LJ beads of diameter σ . The vertices of the icosahedron are connected to adjacent vertices by the same FENE bond as used for polymers. The icosahedral structure was further maintained by imposing an angle of $\theta_0 = \pi/3$ for the 20 equilateral triangle faces, resulting in 60 angles constrained by a harmonic potential $U_{\text{hangle}} = k_{\text{h}\theta}(\theta - \theta_0)^2$ with $k_{\text{h}\theta} = 200 k_B T/\text{rad}^2$. The equilibrium bond length of the FENE bond is 0.961σ , and the radius of a circumscribed sphere around the icosahedron is $R = 0.914\sigma$. This implies a NP to monomer bead diameter ratio of ≈ 1.8 . This value was chosen to mimic the octaaminophenyl-silsesquioxane (OAPS) nanoparticles (diameter ~ 1.8 nm) experimentally studied in paper II.²¹ An attractive site–site interaction between polymer beads and NP beads is modeled as a truncated LJ potential with a cutoff at 2.5σ and attraction strength $\epsilon_{\text{np}} = 2, 4, 8,$ and $32 k_B$; $\epsilon_{\text{np}} > \epsilon$ ensures that NPs remain well dispersed. The number of nanoparticles dispersed in the polymer matrix is low with a number fraction of 0.0005, corresponding to an extremely low NP volume fraction of ~ 0.0014 . We have explicitly verified that this value is small enough to mimic the infinitely dilute “single” NP limit of present theoretical interest, as indicated, for example, by the invariance of the polymer–polymer pair correlation function to NP–polymer attraction strength. The studied degrees of polymerization, N , number of nanoparticles, n_{NP} , number of polymer chains, n_{chain} , and simulation box size, L , are tabulated in Table 1.

Table 1. Simulation Parameters: Chain Degree of Polymerization, Number of Nanoparticles in the Simulation Box, Number of Chains in the Box, and Box Size

| N | n_{NP} | n_{chain} | $L(\sigma)$ |
|-----|-----------------|--------------------|-------------|
| 10 | 5 | 1000 | 22.6 |
| 30 | 15 | 1000 | 32.4 |
| 90 | 45 | 1000 | 46.7 |
| 200 | 100 | 1000 | 60.9 |
| 400 | 100 | 500 | 60.9 |

To prepare the system, NPs are first dissolved in the polymer melt by placing them on a rectangular lattice that spans the simulation box. This corresponds to a well-dispersed initial configuration. Prior to the production run, the box size is equilibrated by performing isothermal–isobaric (NPT) simulations using a Nosé–Hoover thermostat and barostat with reduced pressure $P^* = 0$. Afterward, canonical (NVT) simulations are performed using a Langevin thermostat at reduced temperature $T^* = 1.0$ for the production runs. All simulations were performed at the Oak Ridge Leadership Computing Facility (OLCF) using the LAMMPS software package.^{42,43} The simulations cover the parameter windows $2R/\sigma \approx 2$, $2R/d_T \approx 0.2–0.3$, $R_g/\sigma \approx 2–11$, $N/N_c \approx 0.2–9$, and $\epsilon_{\text{np}}/k_B T = 2, 4, 8,$ and 32 . Based on DFT calculations, $\epsilon_{\text{np}} = 4–6 k_B T$ seems most relevant for our experiments on OAPS in poly(propylene glycol) (PPG) discussed in ref 21. All simulation results are reported in polymer bead LJ units unless otherwise noted.

III.B. Polymer–Nanoparticle Adsorption: Packing Structure and Desorption Time. To characterize NP–polymer adsorption, the site–site pair correlation function between a NP bead and a polymer segment, $g_{\text{np}}(r)$, is

computed. Representative results are shown in Figure 2, along with snapshots of the NP and surrounding polymer melt.

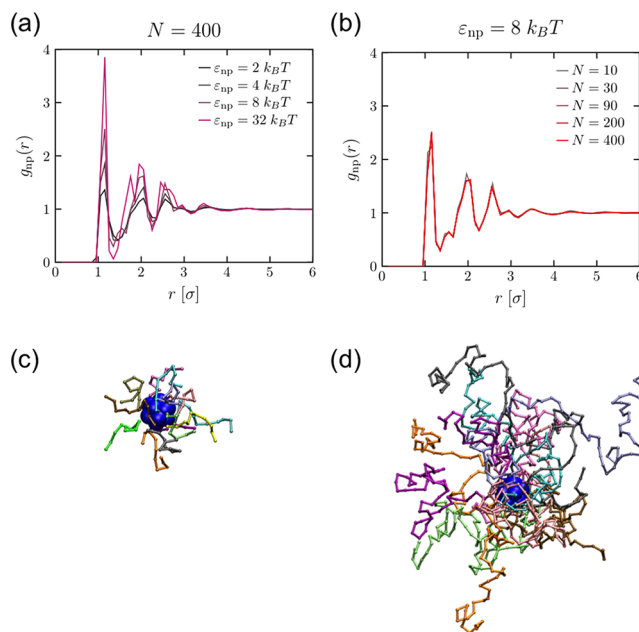


Figure 2. Site–site pair correlation function between a NP bead and polymer segment as a function of separation for (a) $N = 400$ and different values of ϵ_{np} and (b) $\epsilon_{\text{np}} = 8 k_B T$ and different N . Panels (c) and (d) are simulation snapshots of an icosahedron nanoparticle (blue) in a polymer matrix of $N = 10$ and $N = 90$, respectively. The polymer segment–NP interaction $\epsilon_{\text{np}} = 2 k_B T$, and only adsorbed polymers, which are mix-colored chains representing one chain per color, are shown.

We note that $g_{\text{np}}(r)$ peaks at $r \approx \sigma$ with an amplitude that grows with ϵ_{np} , thereby demonstrating the strong cohesion between a NP and the polymer segments. The pair correlation function is essentially independent of N , as expected in dense polymer melts.⁴⁴ The absence of major peaks at larger length scales indicates that the adsorbed segments are likely randomly dangling from the NP surface rather than making compact clusters, supporting the core–shell idea and its nonlinear (starlike) topology⁴⁵ (see Figure 2c,d for simulation snapshots).

The segmental desorption time is quantified by first defining an adsorbed segment as when it is within a certain cutoff distance from a NP—here chosen to be the location of the first minimum of $g_{\text{np}}(r)$ which occurs at $r \sim 1.4\sigma$. The desorption time is then estimated as the average time a given adsorbed segment stays within that spatial region. This analysis is performed by (i) assigning a value of $n(t) = 1$ to all adsorbed segments and $n(t) = 0$ otherwise (repeated for all time steps) and (ii) calculating the time correlation function $Q_D(t) = \langle n(t)n(0) \rangle$ considering only those segments with $n(0) = 1$. The resulting correlation function is fit with a stretched exponential, $Q_0 \exp[-(t/\tau_{\text{des}})^\beta]$, to determine τ_{des} . This analysis describes the simulation data very well with β ranging from 0.36 to 0.58 (see Figure 3a).

For all ϵ_{np} studied, the desorption time only weakly increases with N and saturates above $N = 100$, confirming our expectation that τ_{des} is an essentially N -independent, chemistry-specific quantity (Figure 3b). After saturation, we find a simple Arrhenius form of $\tau_{\text{des}} \propto \exp(a\epsilon_{\text{np}}/k_B T)$ where $a \approx 0.8–1$, a physically intuitive result (plot not shown). Of greater

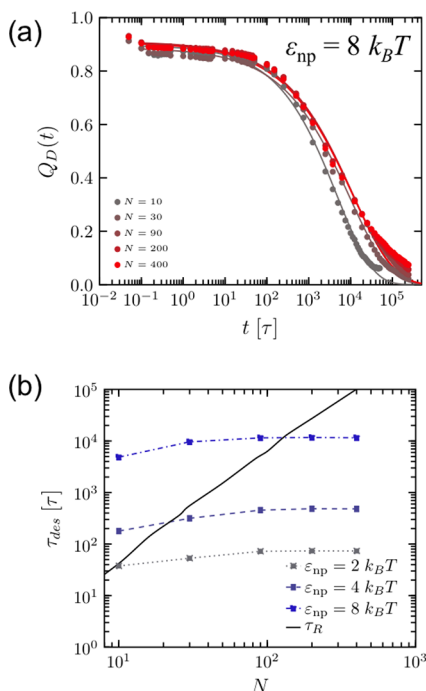


Figure 3. (a) Time correlation function of polymer segment association (for $8 k_B T$ adsorption energy) defined in the text for (from bottom to top) $N = 10, 30, 90, 200,$ and 400 . Curves are a stretched exponential fit of the data, $Q_D(t) = Q_0 \exp[-(t/\tau_{des})^\beta]$. (b) Segmental desorption time (in LJ unit), τ_{des} , as a function of N for (from bottom to top) $\epsilon_{np} = 2, 4,$ and $8 k_B T$. The solid curve is the characteristic Rouse relaxation time of the pure polymer melt from ref 14.

importance is the relationship between the time scales τ_{des} , τ_e , and τ_R . For τ_R we adopt the value of ref 14; we estimate $\tau_e \sim 1.8 \times 10^4 - 9.7 \times 10^4$ based on the time scale where the segmental MSD reaches the tube diameter squared or attains the local reptative subdiffusive exponent of $1/4$ for long chains. The simulation data shows that $\tau_{des} < \tau_R$ for almost all N with $\epsilon_{np} = 2$ and $4 k_B T$, and for large N (≥ 200) with $\epsilon_{np} = 8 k_B T$. Furthermore, τ_{des} is generally smaller than τ_e for $\epsilon_{np} = 2$ and $4 k_B T$ and comparable to τ_e for $\epsilon_{np} = 8 k_B T$. Thus, NP dynamics is expected to be coupled to only the unentangled Rouse-like dynamics of adsorbed chains for $\epsilon_{np} \leq 4 k_B T$ and possibly weakly to entanglements for $\epsilon_{np} = 8 k_B T$.

III.C. Intermediate-Time and Long-Time Dynamics. We now investigate the microscopic dynamics of the NP center-of-mass and polymer segments based on calculation of their mean-square displacement and long-time diffusivity. The polymer dynamics most directly relevant to the vehicle diffusivity is the segmental motion of the adsorbed chains, which is also analyzed.

Figure 4 shows MSD data for the NP, adsorbed segments, and nonadsorbed (“free”) segments at different values of N and ϵ_{np} ; for better clarity and resolution of trends, the same results are replotted in a linear–linear format in the Appendix (Figure 7). For the adsorbed segments, we only include those which remain adsorbed across the displayed time window. Our key findings are now summarized based on examining Figures 4 and 7.

For all cases studied, the NP MSD shows the slowest motion at short times since it is larger than the polymer segments.^{16,19} This trend is similar to that of the adsorbed segments, while the

MSD of free segments is generally the largest, as expected. These short-time behaviors are qualitatively unaffected by N and ϵ_{np} , although the overall mobility is smaller for larger ϵ_{np} since NP–polymer attraction slows down segmental and NP motion.

In contrast, intermediate- and long-time behaviors are qualitatively different depending on N and ϵ_{np} . For small N (≤ 30) and all values of ϵ_{np} , the NP MSD closely agrees with that of the adsorbed segments at long times. This establishes the relevance of the core–shell mechanism where the NP and the adsorbed chains diffuse as a single object. However, for larger N and $\epsilon_{np} \leq 8 k_B T$, the NP motion becomes Fickian at an earlier time than the polymer segments do, and it exhibits a higher diffusivity. This is consistent with τ_{des} being shorter than τ_R for $\epsilon_{np} \leq 8 k_B T$ and indicates the dominance of the vehicle mechanism. The onset of NP Fickian diffusion is shifted to longer times with increasing ϵ_{np} as expected from the vehicle picture. Finally, for $\epsilon_{np} = 32 k_B T$ and $N \geq 100$ the NP MSD does not reach the Fickian diffusion regime as τ_{des} and τ_R are both longer than the simulated time window.

The competition between the core–shell and vehicle controlled dynamics can also be studied via the long-time NP diffusivity, $D_{NP} = \lim_{t \rightarrow \infty} \langle \delta r^2(t) \rangle / 6t$ (Figure 5). At a given ϵ_{np} ,

the NP diffusivity monotonically decreases with polymer chain length for relatively small values of N (≤ 90) and then approaches a plateau at larger N . According to section II, the former is a manifestation of the core–shell dominated regime, while the latter demonstrates a crossover to the vehicle-dominated regime. Note that the N -dependence appears to be the same for $N \leq 30$ for all values of ϵ_{np} , in agreement with our theoretical argument that $D_{core-shell}$ is independent of τ_{des} (except for the overall slowdown) and consistent with the vehicle mechanism of transport. The location of the crossover corresponds to the chain length where the contribution of $D_{vehicle}$ starts to exceed that of $D_{core-shell}$. As expected, this crossover occurs at a larger N value with increasing ϵ_{np} due to weakening of the vehicle diffusion mechanism (recall eqs 12 and 13), which then leads to a wider core–shell dominated window resulting in a stronger apparent N -dependence when $\epsilon_{np} = 8 k_B T$. As a side comment, the N^{-2} scaling of the polymer CM diffusivity for $N > 100$ confirms the emergence of entangled dynamics in the simulated model.¹⁴

III.D. Relevant Polymer Dynamics for the Vehicle Mechanism. We now discuss how NP–polymer attraction strength and degree of entanglement determine which polymer dynamical regime is relevant for the vehicle mechanism and its scaling with τ_{des} (eq 13). As discussed in section II, a convenient approach to test the theoretical expectation is offered by eq 15. It motivates our attempt to find an “optimal” value of the exponent α that leads to a collapse of $D_{NP} \tau_{des}^{1-\alpha}$ at sufficiently large N . To exclude the obvious leading-order effect of an overall slowdown of D_{NP} with increasing ϵ_{np} , a normalized diffusivity, $D_{NP}^* \equiv D_{NP}(\epsilon_{np}) / D_{NP}(\epsilon_{np} = 2 k_B T)$, is adopted and computed at each N .

Results are shown in Figure 6. Interestingly, we see that a nearly constant effective exponent of $\alpha \approx 0.5, 0.56,$ and 0.56 leads to a reasonable collapse of our data when $N \geq 200$. This exponent value strongly suggests that the shorter time unentangled Rouse dynamics is relevant to the vehicle mechanism despite the presence of entanglements ($N/N_e \approx 4.5-9$ for $N \geq 200$). Such a result is intuitive for $\epsilon_{np} = 2$ and $4 k_B T$ for which $\tau_{des} \ll \tau_e$, but a similar trend is also found for ϵ_{np}

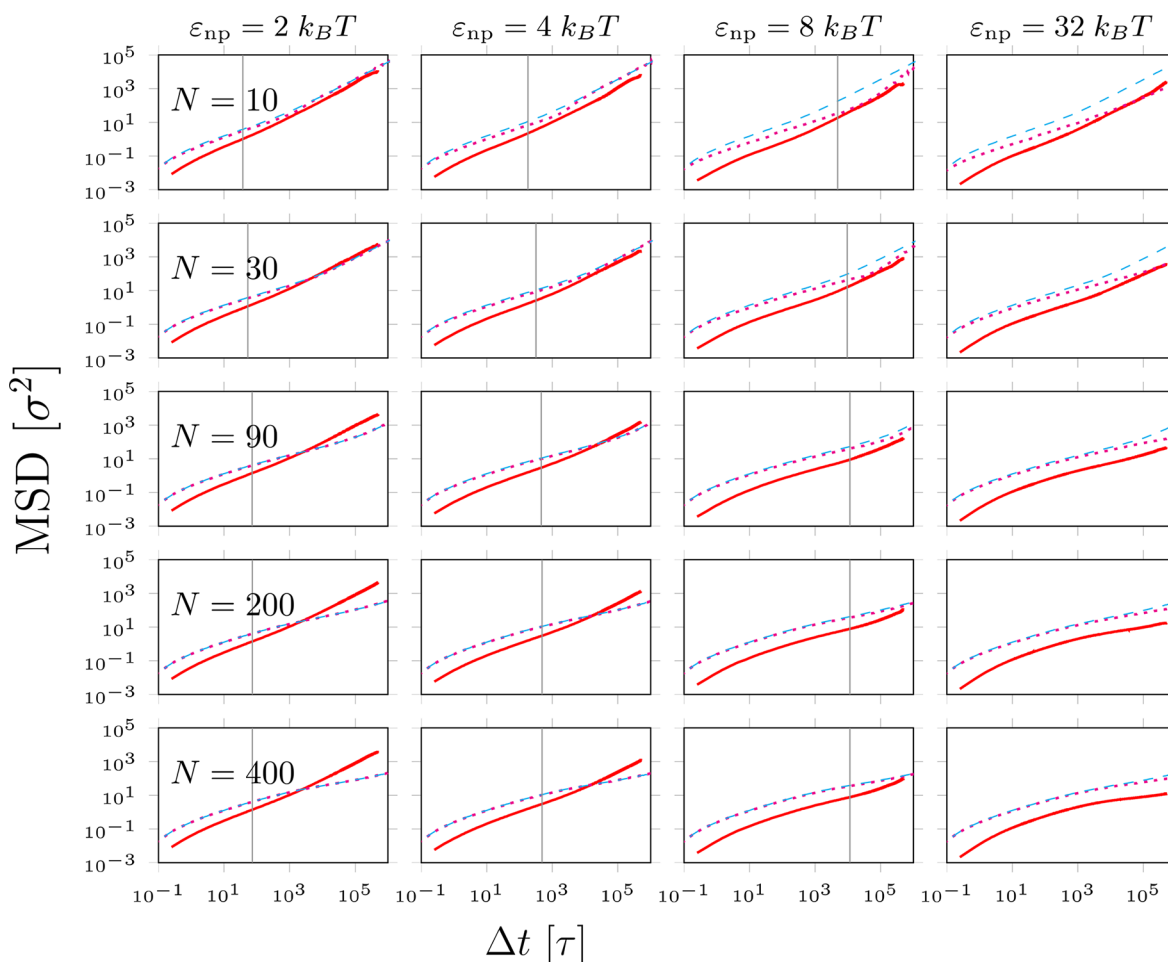


Figure 4. A log–log plot of the mean-squared displacement (MSD) of the NP center-of-mass (red solid curves), free polymer segments (cyan dashed curves) and adsorbed polymer segments (magenta dotted curves) for four values of NP–polymer attraction. The vertical lines for $\epsilon_{\text{np}} = 2, 4,$ and $8 k_B T$ indicate the respective desorption τ_{des} values.

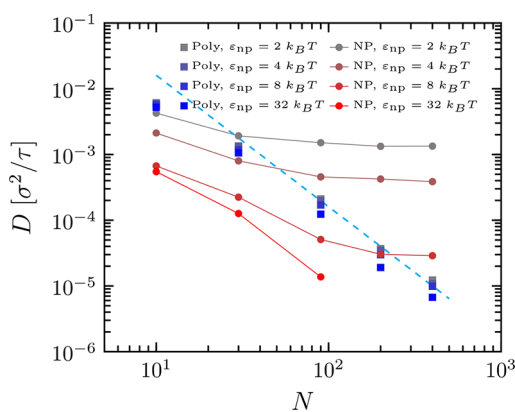


Figure 5. A log–log plot of center-of-mass diffusion coefficients of polymer chains (blue and square data points) and nanoparticles (red to gray circle data points) for different values of N and ϵ_{np} . The NP diffusion constant data decrease from top to bottom as the attraction strength grows. Dashed cyan line represents a quadratic relationship between N and D .

$= 8k_B T$ where $\tau_{\text{des}} \approx \tau_e$ and entanglement effects are present. The slight variation of α for different ϵ_{np} may be due to numerical prefactor differences, the chosen normalization method of D_{NP} , or another second order effect, none of which qualitatively affects the behavior. Thus, up to a significant

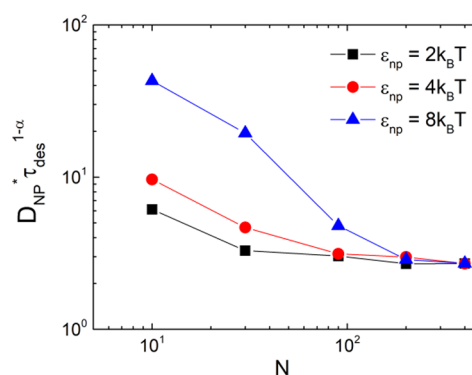


Figure 6. Normalized NP diffusivity, $D_{\text{NP}}^* \equiv D_{\text{NP}}(\epsilon_{\text{np}})/D_{\text{NP}}(\epsilon_{\text{np}} = 2 k_B T)$, multiplied by $\tau_{\text{des}}^{1-\alpha}$ for $\epsilon_{\text{np}} = 2 k_B T$ (black squares), $4 k_B T$ (red circles), and $8 k_B T$ (blue triangles) where α is chosen to be 0.50, 0.56, and 0.56, respectively.

NP–polymer attraction strength of $8 k_B T$, one can understand the N -independent NP diffusivity in the entangled regime solely in terms of the vehicle mechanism controlled by the unentangled segmental dynamics.

IV. SUMMARY

We have theoretically studied the diffusion of a single attractive nanoparticle in unentangled and entangled polymer melts

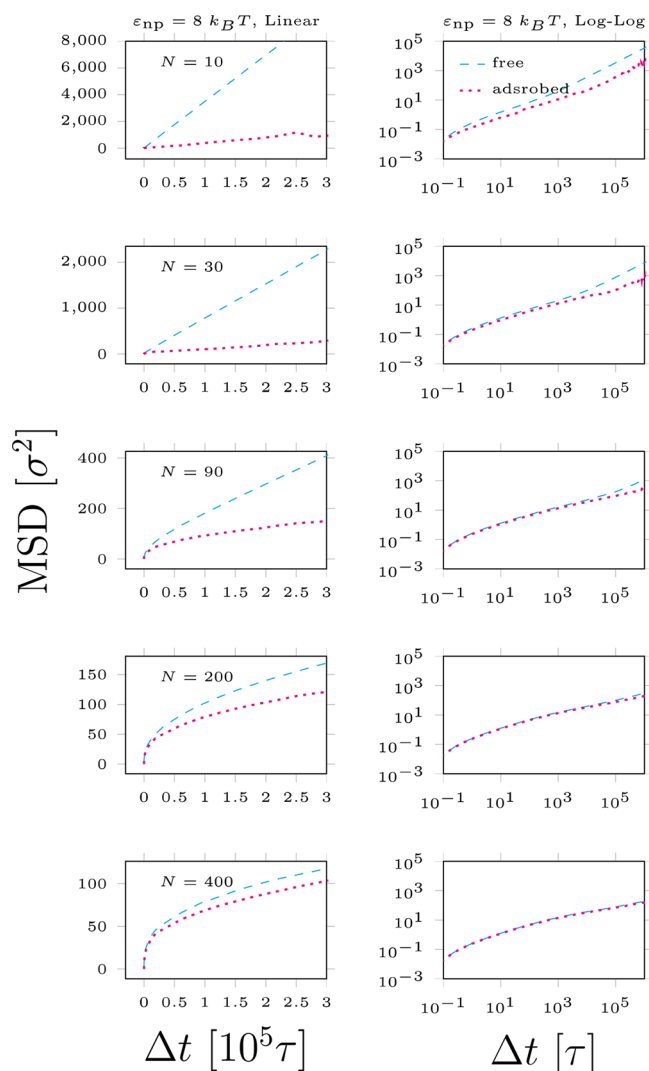


Figure 7. Mean-square displacement of free polymer segments (blue dashed line) and adsorbed segments (pink dotted line) for $\epsilon_{np} = 8 k_B T$ and (from top to bottom) $N = 10, 30, 90, 200,$ and 400 . Left panel displays linear–linear plots, while right panel is the same data on a log–log scale.

based on combining the microscopic “core–shell” and “vehicle” diffusion mechanisms in a dynamic bond percolation theory framework.²⁷ In this approach, the former mechanism (which includes hydrodynamic and nonhydrodynamic contributions) involves NP diffusion when adsorbed chains are dynamically pinned. In conjunction with standard polymer physics melt dynamics models^{28,29} and the SC-GLE theory,¹⁹ a physical picture was constructed for NP diffusivity as a function of chain length and NP–polymer attraction strength. Thinking of the problem in terms of a NP with an effectively larger radius due to an adsorbed polymer layer was argued to be reasonable if the NP size is sufficiently large compared to the matrix chains and the polymer segmental desorption time is longer than the NP diffusion time. The dependence on polymer chain length was analyzed. The NP diffusivity for smaller NPs shows a qualitatively different N -dependence, which initially decreases with N but tends to saturate at large enough N . This behavior is in analogy with what is found for the diffusivity of small repulsive NPs in entangled melts,^{14–19} though for distinct physical reasons related to the adsorption–desorption process.

The theoretically proposed diffusion mechanisms were qualitatively tested against simulations where the segmental desorption time and dynamic MSD’s were calculated. For lower NP–polymer attraction strengths, $\tau_{des} < \tau_e$ and $\epsilon_{np} \leq 4k_B T$, vehicle diffusivity is controlled by the unentangled segmental relaxation. For the higher attraction strength ($8 k_B T$), the desorption and entanglement time scales are comparable, but even in the presence of modest entanglement the NP diffusivity is well captured by the unentangled melt behavior. We do caution that these conclusions depend on nonuniversal system parameters per the theoretical analysis of section II. Future simulations at higher attractions strengths and/or long matrix chains that reverse the $\tau_{des} < \tau_e$ inequality are required to provide further insight into how entanglement physics affects NP transport via the vehicle mechanism. Such simulations require much larger computational resources and are beyond the scope of the present work; future studies will explore this direction. Another major open question is how attractive NP dynamics evolves beyond the infinitely dilute limit where polymer-mediated bridging of nanoparticles⁴⁴ will eventually become important at sufficiently high loadings.

In the companion paper²¹ we present experimental measurements of the diffusion of an ~ 2 nm nanoparticle in a strongly attractive polymer melt. Measurements for large sticky silica nanoparticles are also presented. These data are analyzed using the theoretical concepts discussed here. We find the “core–shell” mechanism dominates for large silica NPs ($R > R_g$). More interestingly, the experiments on small NPs discovered the theoretically predicted crossover from the “core–shell” mechanism at small molecular weight to the “vehicle” mechanism at higher molecular weight. The obtained results help to formulate a broader scenario for the diffusion of nanoparticles in a polymer melt or solution.

■ APPENDIX. SIMULATION DATA FOR MEAN-SQUARE DISPLACEMENTS

The detailed quantitative behavior of the NP, adsorbed segment, and free segment MSDs discussed in section III can be more clearly seen on a linear–linear scale. Figure 7 presents the analogue of Figure 4 in this format.

■ AUTHOR INFORMATION

Corresponding Author

*E-mail kschweiz@illinois.edu (K.S.S.).

ORCID

Jan-Michael Y. Carrillo: 0000-0001-8774-697X

Vera Bocharova: 0000-0003-4270-3866

Bobby G. Sumpter: 0000-0001-6341-0355

Notes

The authors declare no competing financial interest.

■ ACKNOWLEDGMENTS

This work was supported by the U.S. Department of Energy, Office of Science, Basic Energy Sciences, Materials Science and Engineering Division. Simulations were performed at the Center for Nanophase Materials Sciences, which is a US Department of Energy Office of Science User Facility. This research also used resources of the Oak Ridge Leadership Computing Facility at Oak Ridge National Laboratory, which is supported by the Office of Science of the Department of Energy under Contract DE-AC05-00OR22725.

REFERENCES

- (1) Ganesan, V.; Jayaraman, A. Theory and Simulation Studies of Effective Interactions, Phase Behavior and Morphology in Polymer Nanocomposites. *Soft Matter* **2014**, *10*, 13–38.
- (2) Krishnamoorti, R.; Vaia, R. A. Polymer Nanocomposites. *J. Polym. Sci., Part B: Polym. Phys.* **2007**, *45*, 3252–3256.
- (3) Balazs, A. C.; Emrick, T.; Russell, T. P. Nanoparticle Polymer Composites: Where Two Small Worlds Meet. *Science* **2006**, *314*, 1107–1110.
- (4) Lin, C. C.; Parrish, E.; Composto, R. J. Macromolecule and Particle Dynamics in Confined Media. *Macromolecules* **2016**, *49*, 5755–5772.
- (5) Tuteja, A.; Mackay, M. E.; Narayanan, S.; Asokan, S.; Wong, M. S. Breakdown of the continuum Stokes-Einstein relation for nanoparticle diffusion. *Nano Lett.* **2007**, *7*, 1276–1281.
- (6) Grabowski, C. A.; Adhikary, B.; Mukhopadhyay, A. Dynamics of Gold Nanoparticles in a Polymer Melt. *Appl. Phys. Lett.* **2009**, *94*, 021903.
- (7) Kohli, I.; Mukhopadhyay, A. Diffusion of Nanoparticles in Semidilute Polymer Solutions: Effect of Different Length Scales. *Macromolecules* **2012**, *45*, 6143–6149.
- (8) Guo, H. Y.; Bourret, G.; Lennox, R. B.; Sutton, M.; Harden, J. L.; Leheny, R. L. Entanglement-Controlled Subdiffusion of Nanoparticles within Concentrated Polymer Solutions. *Phys. Rev. Lett.* **2012**, *109*, 055901.
- (9) Chapman, C. D.; Lee, K.; Henze, D.; Smith, D. E.; Robertson-Anderson, R. M. Onset of Non-Continuum Effects in Microrheology of Entangled Polymer Solutions. *Macromolecules* **2014**, *47*, 1181–1186.
- (10) Grabowski, C. A.; Mukhopadhyay, A. Size Effect of Nanoparticle Diffusion in a Polymer Melt. *Macromolecules* **2014**, *47*, 7238–7242.
- (11) Alam, S.; Mukhopadhyay, A. Translational and Rotational Diffusions of Nanorods within Semidilute and Entangled Polymer Solutions. *Macromolecules* **2014**, *47*, 6919–6924.
- (12) Mangal, R.; Srivastava, S.; Narayanan, S.; Archer, L. A. Size-Dependent Particle Dynamics in Entangled Polymer Nanocomposites. *Langmuir* **2016**, *32*, 596–603.
- (13) Liu, J.; Cao, D. P.; Zhang, L. Q. Molecular dynamics study on nanoparticle diffusion in polymer melts: A test of the Stokes-Einstein law. *J. Phys. Chem. C* **2008**, *112*, 6653–6661.
- (14) Kalathi, J. T.; Yamamoto, U.; Schweizer, K. S.; Grest, G. S.; Kumar, S. K. Nanoparticle Diffusion in Polymer Nanocomposites. *Phys. Rev. Lett.* **2014**, *112*, 108301.
- (15) Wyart, F. B.; de Gennes, P. G. Viscosity at Small Scales in Polymer Melts. *Eur. Phys. J. E: Soft Matter Biol. Phys.* **2000**, *1*, 93–97.
- (16) Cai, L. H.; Panyukov, S.; Rubinstein, M. Mobility of Nonsticky Nanoparticles in Polymer Liquids. *Macromolecules* **2011**, *44*, 7853–7863.
- (17) Cai, L. H.; Panyukov, S.; Rubinstein, M. Hopping Diffusion of Nanoparticles in Polymer Matrices. *Macromolecules* **2015**, *48*, 847–862.
- (18) Yamamoto, U.; Schweizer, K. S. Theory of Nanoparticle Diffusion in Unentangled and Entangled Polymer Melts. *J. Chem. Phys.* **2011**, *135*, 224902.
- (19) Yamamoto, U.; Schweizer, K. S. Microscopic Theory of the Long-Time Diffusivity and Intermediate-Time Anomalous Transport of a Nanoparticle in Polymer Melts. *Macromolecules* **2015**, *48*, 152–163.
- (20) Dell, Z. E.; Schweizer, K. S. Theory of Localization and Activated Hopping of Nanoparticles in Cross-Linked Networks and Entangled Polymer Melts. *Macromolecules* **2014**, *47*, 405–414.
- (21) Carroll, B.; Bocharova, V.; Carrillo, J.-M.; Kisliuk, A.; Cheng, S.; Yamamoto, U.; Schweizer, K. S.; Sumpter, B. G.; Sokolov, A. P. Diffusion of Sticky Nanoparticles in a Polymer Melt: Crossover from Suppressed to Enhanced Transport. *Macromolecules* **2018**, DOI: 10.1021/acs.macromol.7b02695.
- (22) Kim, S. Y.; Schweizer, K. S.; Zukoski, C. F. Multiscale Structure, Interfacial Cohesion, Adsorbed Layers, and Thermodynamics in Dense Polymer-Nanoparticle Mixtures. *Phys. Rev. Lett.* **2011**, *107*, 225504.
- (23) Kim, S. Y.; Zukoski, C. F. Super- and Sub-Einstein Intrinsic Viscosities of Spherical Nanoparticles in Concentrated Low Molecular Weight Polymer Solutions. *Soft Matter* **2012**, *8*, 1801–1810.
- (24) Griffin, P. J.; Bocharova, V.; Middleton, L. R.; Composto, R. J.; Clarke, N.; Schweizer, K. S.; Winey, K. I. Influence of the Bound Polymer Layer on Nanoparticle Diffusion in Polymer Melts. *ACS Macro Lett.* **2016**, *5*, 1141–1145.
- (25) Maitra, A.; Heuer, A. Cation Transport in Polymer Electrolytes: A Microscopic Approach. *Phys. Rev. Lett.* **2007**, *98*, 227802.
- (26) Diddens, D.; Heuer, A.; Borodin, O. Understanding the Lithium Transport within a Rouse-Based Model for a PEO/LiTFSI Polymer Electrolyte. *Macromolecules* **2010**, *43*, 2028–2036.
- (27) Druger, S. D.; Ratner, M. A.; Nitzan, A. Generalized Hopping Model for Frequency-Dependent Transport in a Dynamically Disordered Medium, with Applications to Polymer Solid Electrolytes. *Phys. Rev. B: Condens. Matter Mater. Phys.* **1985**, *31*, 3939–3947.
- (28) Doi, M.; Edwards, S. F. *The Theory of Polymer Dynamics*; Clarendon Press: 1988.
- (29) Rubinstein, M.; Colby, R. H. *Polymer Physics* OUP Oxford; Oxford University Press: Oxford, 2003.
- (30) Doi, M. Relaxation Spectra of Nonlinear Polymers. *Polym. J.* **1974**, *6*, 108–120.
- (31) Daoud, M.; Degennes, P. G. Some Remarks on the Dynamics of Polymer Melts. *J. Polym. Sci., Polym. Phys. Ed.* **1979**, *17*, 1971–1981.
- (32) Klein, J.; Fletcher, D.; Fetters, L. J. Dynamics of Entangled Star-Branched Polymers. *Faraday Symp. Chem. Soc.* **1983**, *18*, 159–171.
- (33) de Gennes, P. G. *Scaling Concepts in Polymer Physics*; Cornell University Press: 1979.
- (34) van Zon, A.; de Leeuw, S. W. A Rouse Model for Polymer Electrolytes. *Electrochim. Acta* **2001**, *46*, 1539–1544.
- (35) Gibbs, J. H.; Dimarzio, E. A. Nature of the Glass Transition and the Glassy State. *J. Chem. Phys.* **1958**, *28*, 373–383.
- (36) Hofmann, M.; Kresse, B.; Heymann, L.; Privalov, A. F.; Willner, L.; Fatkullin, N.; Aksel, N.; Fujara, F.; Rossler, E. A. Dynamics of a Paradigmatic Linear Polymer: A Proton Field-Cycling NMR Relaxometry Study on Poly(ethylene-propylene). *Macromolecules* **2016**, *49*, 8622–8632.
- (37) Mordvinkin, A.; Saalwachter, K. Microscopic Observation of the Segmental Orientation Autocorrelation Function for Entangled and Constrained Polymer Chains. *J. Chem. Phys.* **2017**, *146*, 094902.
- (38) Takahashi, K. Z.; Nishimura, R.; Yasuoka, K.; Masubuchi, Y. Molecular Dynamics Simulations for Resolving Scaling Laws of Polyethylene Melts. *Polymers* **2017**, *9*, 24.
- (39) Qin, J.; Milner, S. T. Tube Dynamics Works for Randomly Entangled Rings. *Phys. Rev. Lett.* **2016**, *116*, 068307.
- (40) Kremer, K.; Grest, G. S. Dynamics of Entangled Linear Polymer Melts - a Molecular-Dynamics Simulation. *J. Chem. Phys.* **1990**, *92*, 5057–5086.
- (41) Auhl, R.; Everaers, R.; Grest, G. S.; Kremer, K.; Plimpton, S. J. Equilibration of Long Chain Polymer Melts in Computer Simulations. *J. Chem. Phys.* **2003**, *119*, 12718–12728.
- (42) Plimpton, S. Fast Parallel Algorithms for Short-Range Molecular-Dynamics. *J. Comput. Phys.* **1995**, *117*, 1–19.
- (43) Brown, W. M.; Wang, P.; Plimpton, S. J.; Tharrington, A. N. Implementing molecular dynamics on hybrid high performance computers - short range forces. *Comput. Phys. Commun.* **2011**, *182*, 898–911.
- (44) Hooper, J. B.; Schweizer, K. S. Contact Aggregation, Bridging, and Steric Stabilization in Dense Polymer-Particle Mixtures. *Macromolecules* **2005**, *38*, 8858–8869.
- (45) Hall, L. M.; Stevens, M. J.; Frischknecht, A. L. Effect of Polymer Architecture and Ionic Aggregation on the Scattering Peak in Model Ionomers. *Phys. Rev. Lett.* **2011**, *106*, 127801.